Structural Changes of Phenylalanine 338 and Histidine 447 Revealed by the Crystal Structures of Tabun-Inhibited Murine Acetylcholinesterase[†,‡]

Fredrik Ekström,* Christine Akfur, Anna-Karin Tunemalm, and Susanne Lundberg

Swedish Defense Research Agency, Division of NBC Defense, S-901 82 Umeå, Sweden

Received July 5, 2005; Revised Manuscript Received September 9, 2005

ABSTRACT: Organophosphorus compounds (OPs) interfere with the catalytic mechanism of acetylcholinesterase (AChE) by rapidly phosphorylating the catalytic serine residue. The inhibited enzyme can at least partly be reactivated with nucleophilic reactivators such as oximes. The covalently attached OP conjugate may undergo further intramolecular dealkylation or deamidation reactions, a process termed "aging" that results in an enzyme considered completely resistant to reactivation. Of particular interest is the inhibition and aging reaction of the OP compound tabun since tabun conjugates display an extraordinary resistance toward most reactivators of today. To investigate the structural basis for this resistance, we determined the crystal structures of *Mus musculus* AChE (mAChE) inhibited by tabun prior to and after the aging reaction. The nonaged tabun conjugate induces a structural change of the side chain of His447 that uncouples the catalytic triad and positions the imidazole ring of His447 in a conformation where it may form a hydrogen bond to a water molecule. Moreover, an unexpected displacement of the side chain of Phe338 narrows the active site gorge. In the crystal structure of the aged tabun conjugate, the side chains of His447 and Phe338 are reversed to the conformation found in the apo structure of mAChE. A hydrogen bond between the imidazole ring of His447 and the ethoxy oxygen of the aged tabun conjugate stabilizes the side chain of His447. The displacement of the side chain of Phe338 into the active site gorge of the nonaged tabun conjugate may interfere with the accessibility of reactivators and thereby contribute to the high resistance of tabun conjugates toward reactivation.

Acetylcholinesterase (AChE)[1] terminates cholinergic neurotransmission by catalyzing the hydrolysis of the neurotransmitter acetylcholine (ACh). AChE is a highly efficient enzyme, with a turnover number of about 10^4 s^{-1}. The catalytic site of AChE is found close to the base of a narrow active site gorge which penetrates about 20 Å into the enzyme (*1*). The catalytic triad comprises the residues Ser203, Glu334, and His447 that together with Trp86 bind the trimethylammonium group of acetylcholine as acyl transfer to Ser203 is initiated.

AChE is the primary target for different organophosphorus compounds (OPs) that irreversibly inhibit the enzyme. Organophosphorus pesticides such as paraoxon and methamidophos are used in modern agriculture, and the chemical nerve agents continue to be a threat to the society due to their possible use during military conflicts or in terrorist acts (*2*, *3*). The broad distribution of OPs causes several hundred thousands of intoxications each year, of which some are fatal (*4*, *5*). Organophosphorus compounds inhibit AChE by forming stable alkyl phosphate or phosphoramidate conjugates that are covalently attached to the catalytic serine residue, exemplified by tabun in Scheme 1. The function of the enzyme can be restored by removal of the phosphorus conjugate, a process termed reactivation. One important treatment of OP intoxications is the reactivation of inhibited AChE with oxime-based reactivators, such as obidoxime, HI-6, and pralidoxime. The efficiency of these molecules is highly dependent on the chemical nature of the AChE−OP conjugate. For instance, HI-6 is a potent reactivator of AChE inhibited by sarin whereas it is considered a poor reactivator of AChE inhibited by tabun (*6*, *7*). The picture is further complicated by the fact that the R_P and S_P enantiomers of the OP conjugate exhibit different resistance toward reactivation (*8*, *9*). Of the chemical nerve agents, tabun conjugates are notably resistant toward reactivation with most oximes of today (*6*, *7*, *10*).

After inhibition, the phosphorus conjugate may undergo further intramolecular modifications, a process termed "aging" that normally involves dealkylation or deamidation of

[†] This work was supported by the Swedish Armed Forces Research and Technology Program.

[‡] Protein Data Bank entry codes are 2C0Q and 2C0P for the structures of nonaged and aged tabun-inhibited AChE, respectively.

* Corresponding author. E-mail: fredrik.ekstrom@foi.se. Telephone: +46-90-106815. Fax: +46-90-106809.

[1] Abbreviations: AChE, acetylcholinesterase; eAChE, *Electrophorus electricus* acetylcholinesterase; DTNB, 5,5′-dithiobis(2-nitrobenzoic acid); DFP, diisopropyl phosphorofluoridate; Echothiophate, *O*,*O*′-diethyl *S*-(2-trimethylaminoethyl) phosphorothiolate iodide; HI-6, 1-(2-hydroxyiminomethylpyridinium)-1-(4-carboxyimino)pyridinium dimethyl ether dichloride; hAChE, *Homo sapiens* acetylcholinesterase; paraoxon, diethyl *p*-nitrophenyl phosphate; mAChE, *Mus musculus* acetylcholinesterase; methamidophos, *O*,*S*-dimethyl phosphoramidothiolate; OP, organophosphorus compounds; Sarin, methylethyl methylphosphonofluoridate; Soman, 1,2,2-trimethylpropyl methylphosphonofluoridate; tabun, ethyl *N*,*N*-dimethylphosphoramidocyanidate; TMB-4, 1,1′-trimethylenebis(4-formylpyridinium bromide) dioxime; *Tc*AChE, *Torpedo californica* acetylcholinesterase; TMTFA, *m*-(*N*,*N*,*N*-trimethylammonio)-2,2,2-trifluoroacetophenone; VX, *O*-ethyl *S*-(2-isopropylaminoethyl) methylphosphonothiolate. The sequence numbering of mAChE is used throughout this paper when amino acids of any AChE are discussed.

10.1021/bi051286t CCC: $33.50
Published on Web 12/07/2005

Scheme 1: Scheme Describing the Inhibition of AChE by Tabun and the Two Aging Pathways That May Be Possible for the Tabun Conjugate

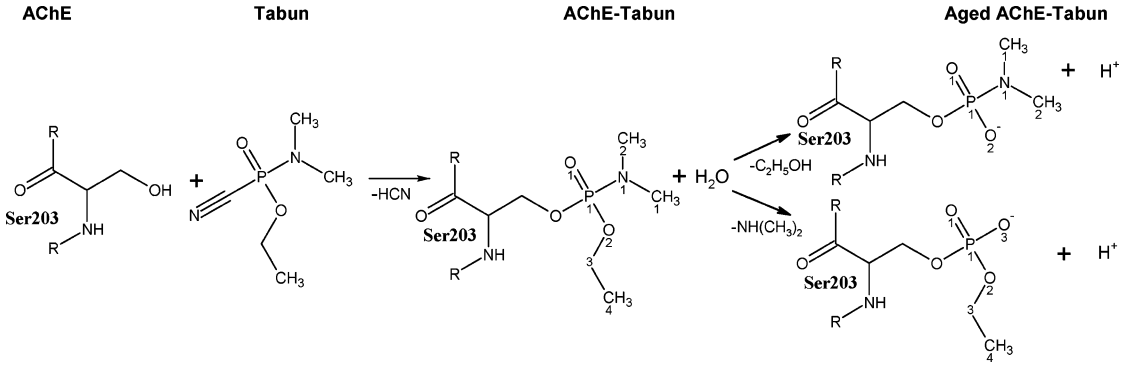

the AChE−OP conjugate (*11*−*15*). Prior to aging, the activity of AChE may be restored by reactivation whereas an aged enzyme is truly irreversibly inhibited. Consequently, the aging process is an important aspect that limits the effectiveness of therapeutic reactivators. The rate by which OP-inhibited AChE undergoes the aging process depends on the organophosphorus moiety as well as the source and sequence of the enzyme. For instance, the rate of aging of human AChE (hAChE) inhibited by soman is affected by the substitutions Glu202Gln and Phe338Ala whereas the same substitutions have a relatively small effect on the aging of hAChE inhibited by tabun (*16*−*19*).

The aging process of AChE inhibited by sarin, soman, and VX yields a stable anionic methylphosphonylated (MeO_2P) AChE reaction product (*14*, *20*), whereas two alternative pathways may be possible for phosphoroamidates (P−N agents) such as tabun (*21*). Mass spectrometric analysis of reaction products of tabun-inhibited AChE strongly supports an aging reaction that proceeds through a P−N scission and elimination of the dimethylamine moiety of the tabun conjugate to yield an anionic ($OEtO_2P$) AChE end product (*18*, *22*).

Crystal structures of the aged form of *Torpedo californica* acetylcholinesterase (*Tc*AChE) treated with sarin, soman, DFP, and VX have been determined, as well as the nonaged form of the VX conjugate (*20*, 23). In addition, the structures of the related enzyme butyrylcholinesterase (BChE) inhibited by DFP and echothiophate have been determined (*24*). Although reactivation kinetics in combination with site-directed mutagenesis have proven a valuable tool to investigate the mechanism of oxime reactivation (*8*, *9*, *25*−*28*), the structural basis for the resistance of tabun conjugates toward reactivation is unknown. To address this question, we present the crystal structures of acetylcholinesterase inhibited by tabun, prior to and after the aging reaction.

MATERIALS AND METHODS

Cloning and Expression of mAChE. Recombinant "wild-type" AChE from mouse (mAChE) was amplified by PCR, and the fragments were inserted into a pcDNA3.1 expression vector (Invitrogene). The inserted open reading frame contained the native N-terminal secretion signal while the C-terminal part of the protein was truncated at position 549, to create a mAChE expression vector similar to vectors previously described (*29*, *30*). HEK-293F cells (Invitrogene) were maintained in Dulbecco's DMEM medium supplemented with 10% fetal calf serum and appropriate antibiotics. Cells (4×10^6/100 mm plate) were transfected with 25 μg of DNA−calcium phosphate coprecipitate (Invitrogene). Transfected clones were selected by incubation with media containing geneticin (Invitrogene) at a concentration of 0.5 mg/mL. When cell death subsided, individual clones were manually transferred to 24 well plates. Clones with high expression of AChE were expanded and transferred to suspension cultures maintained in serum-free FreeStyle media (Invitrogene) for large-scale protein production.

Purification of mAChE. A purification method based on affinity chromatography and size exclusion chromatography (SEC) was employed. Typically, supernatants of media containing ∼30 mg of AChE were pooled and centrifuged at 6500*g* for 30 min. An appropriate amount of procainamide hydrochloride (Sigma), immobilized to epoxy-activated Sepharose 6B (Amersham Biosciences), was incubated with the cleared protein suspension for 10 min. After a brief centrifugation the procainamide Sepharose was transferred to a XK26 column (Amersham Biosciences). Following extensive washing with buffer A [1 mM MES, pH 6.5, 50 mM NaCl, 1 mM poly(ethylene glycol) 600] the protein was eluted in the same buffer supplemented with 50 mM procainamide. The protein was concentrated with centricons (Amicon) and further purified on a HiLoad 16/60 Superdex 200 column (Amersham Biosciences) equilibrated in buffer A. Fractions containing mAChE were detected using a modified Ellman assay (*31*) in E-buffer composed of 100 mM sodium phosphate, pH 8.0, and 0.1% Triton X-100.

Crystal Screening and Refinement of Crystallization Parameters. Crystal screening experiments were performed at 4 °C using hanging drops and the vapor diffusion method. Initial screens explored low molecular weight poly(ethylene glycol)s and a pH range of 6−8 with different sizes of the drop (1−4 μL), ratios between well solution and protein solution (1:1 and 1:2), and protein concentrations (5.5−22 mg/mL). Crystals were grown starting with a protein concentration of ∼22 mg/mL in 27−31% (v/v) poly(ethylene glycol) monomethyl ether 750 and 50−100 mM HEPES, pH 6.8−7.4. The ratio between the protein and the mother liquid was 1:1, and the drop sizes were 2−4 μL. To generate the nonaged tabun conjugates, crystals of mAChE were incubated with tabun at a concentration of ∼0.5 mM for 1 h prior to flash freezing in liquid nitrogen. The aged tabun conjugates were generated by crystallization of mAChE in a mother liquid supplemented with 1 mM tabun. To ensure

that the conjugate was indeed aged, the cocrystals were incubated in the mother liquid for at least 4 weeks prior to flash freezing in liquid nitrogen.

Activity, Inhibition, and Reactivation of Crystalline and Noncrystalline AChE. The limiting rate (V_{max}) and the Michaelis−Menten constant (K_m) of AChE were determined by measurements of the enzyme activity at different concentrations of the substrate acetylthiocholine iodide. Lineweaver−Burk plots were generated with the GraFit 5.0 program package (Erithacus Software Ltd.). The apparent catalytic first-order rate constant (k_{cat}) was determined from V_{max}, and the numbers of active sites were established in titrations with the fast-reacting stereoisomers of soman (*32*). The presented values of K_m and k_{cat} are the mean values of four independent experiments that deviated less than 15%. Complete inhibition of the soaked and cocrystallized mAChE crystals was verified by measurement of residual activity on dissolved crystals. Excess inhibitor was removed by washing the crystals several times in X-buffer composed of 28% (v/v) poly(ethylene glycol) monomethyl ether 750 and 100 mM HEPES, pH 7.2. Residual activity was determined by dissolving the crystals in E-buffer containing a small amount of exogenously added AChE. With this procedure it is possible to verify that the crystals are completely inhibited and that no inhibitor entrapped in the crystals interferes with the assay. The inhibited crystals were further characterized in reactivation experiments. Several (four to five) AChE crystals originating from the same drop were inhibited in X-buffer supplemented with 0.5 mM tabun. After incubation for 1 h and 2 weeks, crystals were washed in X-buffer and dissolved in 40 μL of E-buffer. At this point, 20 μL of the sample was used to quantify the amount of dissolved AChE (see below) whereas the remaining 20 μL was subjected to a buffer exchange on a NAP-5 column (Amersham Biosciences) to remove any traces of residual inhibitor. Following incubation at 30 °C for 2 h in E-buffer supplemented with TMB-4, the restored activity was determined and compared to a control sample of noninhibited crystals. To estimate the quantity of AChE in the samples, an appropriate amount of the AChE solution was separated by SDS−PAGE gel electrophoresis (Bio-Rad). The gel was silver stained, and the relative amount of loaded AChE was estimated by visual inspection of the gel. The restored activity was normalized according to the quantity of AChE in the samples. To investigate the reactivation of noncrystalline AChE inhibited by tabun, purified AChE was inhibited in X-buffer supplemented with 0.5 mM tabun for 1 h. Excess of inhibitor was removed by a buffer exchange on a NAP-5 column. An appropriate amount of AChE was transferred to E-buffer supplemented with 2 mM TMB-4. After incubation at 30 °C for 2 h, the restored activity was determined and compared to a control sample of noninhibited AChE.

Collection, Processing, and Refinement of Diffraction Data. Crystals were flash-frozen in liquid nitrogen, and X-ray diffraction data were collected at 100 K at the MAXlab synchrotron, beamline I711, on a MAR Research CCD detector (Lund, Sweden). Images were collected with an oscillation angle of 1.0° per exposure, and the total oscillation range covered at least 160° per data set. Intensity data were indexed and integrated with XDS (*33*) and scaled using Scala (*34*). The structure was solved using rigid body refinement with the apo structure of mAChE as a starting model (*35*). Further crystallographic refinement was carried out using restrained isotropic *B*-factor refinement as implemented in the program Refmac5 (*36*). Refinement included 98% of the data whereas the remaining 2% was randomly excluded and used to follow the progress of the refinement with R_{free} (*37*). Several rounds of refinement were performed, alternating with manual rebuilding of the model after visualization of $2|F_o| - |F_c|$ and $|F_o| - |F_c|$ maps using the program O (*38*). The quality of the final model was evaluated using PROCHECK (*39*) and WHATCHECK (*40*).

RESULTS

Characterization of Crystalline and Noncrystalline mAChE. To investigate if the constraints of the crystal lattice affect the basic catalytic parameters of the enzyme, we determined the Michaelis−Menten constant (K_m) and the turnover number (k_{cat}) of mAChE prior to and after crystallization. The K_m value of AChE derived from dissolved crystals was determined to 60 μM whereas the turnover number reached 3000 s^{-1}. The corresponding parameters for noncrystallized mAChE show only minor deviations with a K_m of 50 μM and a k_{cat} of 3500 s^{-1} (plots are included in the Supporting Information, Figure 1). The enzyme was further investigated with respect to the reactivation of the inhibited enzyme. Crystals were incubated with tabun for 1 h and 2 weeks prior to dissolution in a buffer supplemented with the oxime TMB-4. The reactivation reaction was allowed to proceed for 2 h at a temperature of 30 °C prior to measurements of the restored AChE activity. As a control, noninhibited crystals were used. The amount of AChE in the samples was quantified by gel electrophoresis followed by a visual estimation of the relative amounts of loaded AChE (gel included in the Supporting Information, Figure 2). The efficiency of TMB-4 on AChE−tabun conjugates derived from crystals inhibited for 1 h reached 62%. As a control, the same experiment was performed on noncrystalline AChE; in this case the efficiency of TMB-4 was 67%. Repeating the experiments on AChE crystals that were incubated with tabun for 2 weeks resulted in a low efficiency of the reactivation (estimated to be less than 5%).

Crystallization, X-ray Diffraction, and Data Processing. Diffraction quality crystals of mAChE were grown in 27−31% (v/v) poly(ethylene glycol) monomethyl ether 750 and 50−100 mM HEPES, pH 6.8−7.4. The first crystal nucleus appeared 4 days after setup, and the crystals continued to grow for another 5−6 days to a final size of about 0.2 × 0.2 × 0.6 mm. The space group was determined to $P2_12_12_1$, and the crystals diffracted to a *d*-spacing of 2.5 Å (Table 1). The initial maps were of good quality, and the phosphorus atoms of the conjugates were clearly visible as a density feature at a contour level of $>9\sigma$ in the initial $|F_o| - |F_c|$ map.

Structure of mAChE−Tabun Prior to Aging. The 2.5 Å structure of mAChE in complex with nonaged tabun reveals a conjugate that is coordinated by an array of stabilizing forces (Figure 1). The phosphorus atom is found at a covalent bonding distance of 1.6 Å from the Ser203Oγ atom. The O1 phosphonyl oxygen is located on hydrogen-bonding distances of the main chain amide nitrogen of Gly121 (2.8 Å), Gly122 (2.7 Å), and Ala204 (2.9 Å). The phosphonyl ethoxy moiety is aligned along the axis of the active site

Table 1: Crystallographic Data Collection and Refinement Statistics

	nonaged tabun−AChE	aged tabun−AChE
data collection		
unit cell dimensions (Å)	79.62 × 112.94 × 226.16	79.02 × 110.88 × 226.38
resolution range (Å)	29.2−2.5 (2.64−2.5)	29.0−2.5 (2.64−2.50)
total no. of reflections	442401 (63864)	511382 (74384)
unique reflections	71021 (10295)	69074 (9958)
completeness (%)	99.6 (100.0)	99.3 (99.0)
multiplicity	6.2 (6.2)	7.4 (7.5)
R_{merge}[a]	0.093 (0.588)	0.074 (0.513)
mean(I)/SD(I)	14.4 (3.3)	17.6 (4.9)
refinement		
R-factor[b]/R_{free}[c] (%)	19.6/24.6	18.2/22.0
B-factor[d] (Å^2)	44.4/49.2	47.3/52.5
RMS from ideality		
bond lengths (Å)	0.013	0.012
bond angle (deg)	1.464	1.377

[a] $R_{merge} = (\Sigma|I - \langle I\rangle|)/\Sigma I$, where I is the observed intensity and $\langle I\rangle$ is the average intensity obtained after multiple observations of symmetry-related reflections. [b] R-factor $= (\Sigma||F_o| - |F_c||)/\Sigma|F_o|$, where F_o are observed and F_c are calculated structure factors. [c] R_{free} uses 2% randomly chosen reflections defined in Brunger et al. (*20*). [d] B-factor is the mean factor for protein main chain A/B.

gorge with a water molecule (Z134) at hydrogen-bonding distance (3.2 Å) of the O2 oxygen atom. The C3 atom of the ethoxy moiety is found at a distance of 3.5 Å from Gly121Cα whereas the C4 atom is coordinated by Phe338Cζ (3.6 Å) and Gly121C (3.6 Å). The dimethylamine moiety of the nonaged tabun conjugate could not be unambiguously resolved in the electron density map. Nevertheless, the only position consistent with the electron density map is to refine the dimethylamine moiety adjacent to the acyl pocket (Figure 1). The C1 methyl group is coordinated with a distance of 3.3 Å to Phe338Cε1 and 3.5 Å to Phe295Cζ whereas the C2 methyl group is coordinated by Trp236Cζ3 (3.6 Å) and Phe297Cζ (3.6 Å).

In the structure of the nonaged tabun conjugate, the side chain of His447 undergoes a movement (3.5 Å for the Nε2 atom) toward Phe338 and uncouples the catalytic triad by a disruption of the hydrogen bond between His447Nδ1 and Glu334Oε1. The His447 Nδ1 atom is located at a hydrogen-bonding distance from a water molecule (2.8 Å). Furthermore, the side chain of Phe338 undergoes a dislocation of 3.0 Å (Phe338Cζ) toward the phenyl ring of Tyr124. Since the $2|F_o| - |F_c|$ electron density is rather weak for the side chain of Phe338, we collected one additional data set of mAChE inhibited by tabun (data not shown). Although these data have lower resolution, the conformations of Phe338 and His447 are clearly defined in the electron density map. The displacements of Phe338 and His447 are the only significant structural changes of the polypeptide chain that are observed

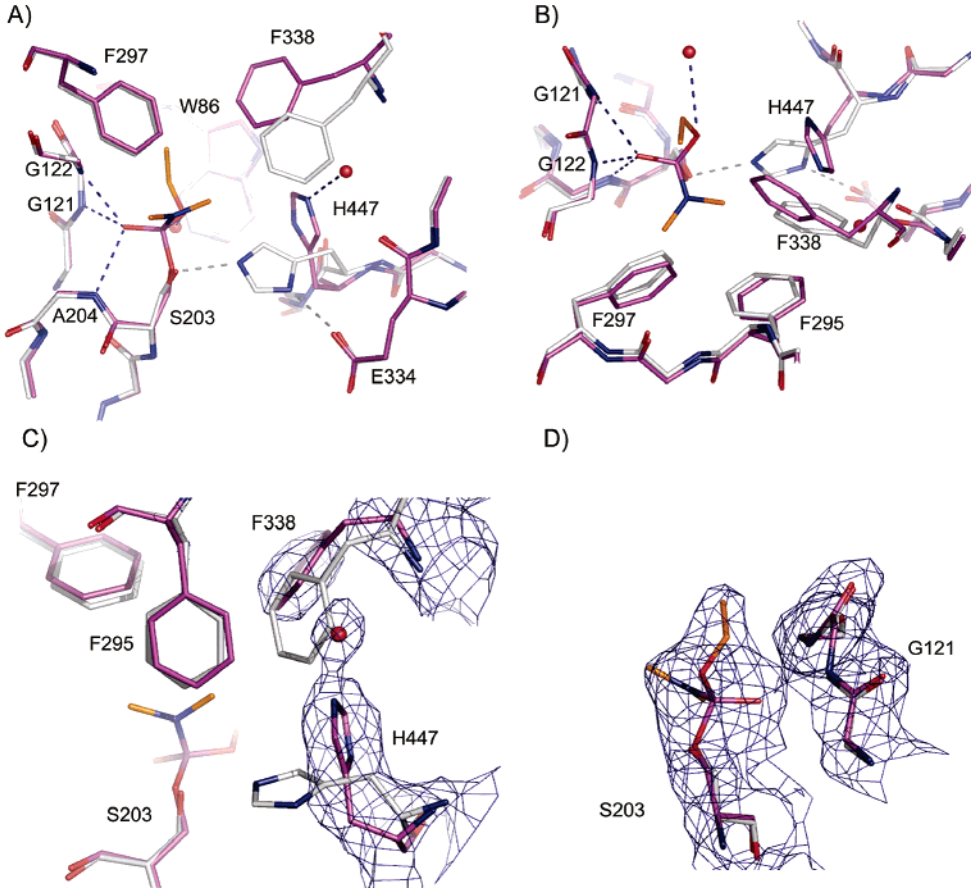

FIGURE 1: Structural alignment of the nonaged tabun conjugate (magenta) and the apo structure of mAChE (gray; PDB entry 1J06). The carbon atoms of the tabun conjugate are shown in orange, the phosphorus atom is in magenta, and oxygen and nitrogen atoms are in red and blue, respectively. Hydrogen bonds are shown as blue or gray dashed lines. (A) The tabun conjugate viewed from the acyl pocket. For clarity, Phe295 is omitted. (B) Rotation of (A) 90° along the x-axis gives the view of the phosphorus conjugate from the entrance of the active site gorge. (C) Electron density ($2|F_o| - |F_c|$) map (blue) contoured at 1σ covering the side chains of His447 and Phe338. (D) $2|F_o| - |F_c|$ map contoured at 1σ showing the nonaged tabun conjugate.

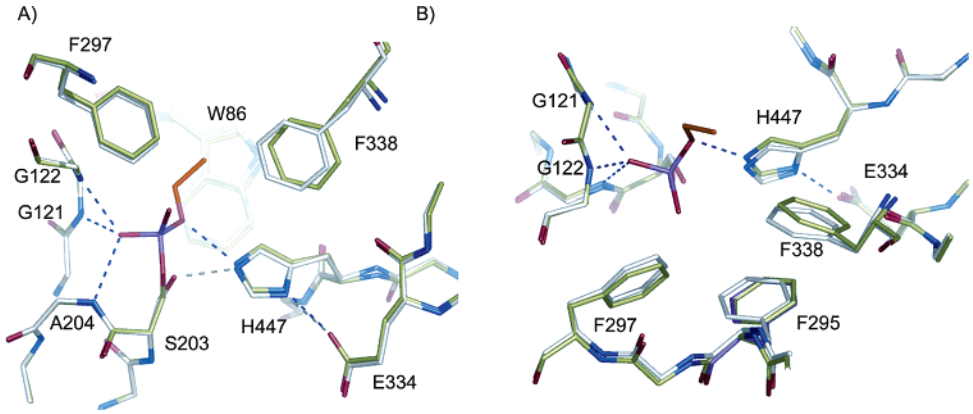

FIGURE 2: Structural alignment of the aged tabun conjugate (green) and the apo form of mAChE (gray; PDB entry 1J06). The aged tabun conjugate is shown in orange and the phosphorus atom in magenta whereas oxygen and nitrogen atoms are shown in red and blue, respectively. Hydrogen bonds are shown as blue or gray dashed lines. (A) The tabun conjugate viewed from the acyl pocket. For clarity, Phe295 is omitted. (B) Rotation of (A) 90° along the *x*-axis gives the view of the phosphorus conjugate from the entrance of the active site gorge.

in the nonaged structure of mAChE inhibited by tabun, and the overall fold is very similar to the apo structure of mAChE (*35*).

Structure of the mAChE−Tabun Aging Product. Features of the initial electron density map support an aging pathway that proceeds through elimination of the dimethylamine moiety. This observation is in agreement with mass spectrometric analysis of tabun-inhibited AChE (*18*, *22*). For the refinement of the aged tabun conjugate, the dimethylamine moiety was replaced with the oxygen O3. The overall coordination of the aged tabun conjugate is similar to the nonaged tabun conjugate (Figure 2). Consequently, the O1 phosphonyl oxygen is located within hydrogen-bonding distances of the main chain amide nitrogen of Gly121 (2.7 Å), Gly122 (2.6 Å), and Ala204 (3.0 Å). The O3 oxygen is adjacent to the acyl pocket with a distance of 4.1 Å to Phe295Cζ and 3.7 Å to Phe297Cζ. Comparable to the nonaged structure, the ethoxy chain is aligned along the axis of the active site gorge whereas the side chains of Phe338 and His447 are reversed to the position found in the apo structure of mAChE. In this conformation, His447 is immobilized by a strong 2.7 Å hydrogen bond between the Nϵ2 atom of the imidazole ring and the O2 oxygen of the ethoxy moiety of the tabun conjugate. The C3 atom of the ethoxy chain is coordinated at a distance of 3.8 Å of Gly121Cα, and the ethoxy C4 atom is without any close interaction partners.

DISCUSSION

Although acetylcholinesterase inhibited by tabun is highly resistant toward most therapeutically used oximes, high concentrations of certain oximes such as TMB-4 can be used for studies of reactivation kinetics (*10*). This encourages trials designed to investigate the reactivation of AChE that has been inhibited by tabun within the constraints of the crystal packing. Reactivation of nonaged tabun conjugates formed in crystalline and noncrystalline AChE results in a comparable efficiency of 62% and 67% for the crystalline and noncrystalline samples, respectively. Repeating the experiments with crystals incubated for 2 weeks prior to dissolution and reactivation resulted in a low efficiency of the reactivation (estimated to be less than 5%), as expected from nearly completely aged tabun conjugates. Since reflection data of mAChE inhibited by tabun were collected at two different time points, 1 h and 4 weeks after inhibition, these results confirm that the structures presented correspond to nonaged and aged AChE−tabun conjugates, respectively.

The nonaged conjugate of mAChE inhibited by tabun is coordinated with the O1 oxygen atom in the oxyanion hole, the dimethylamine moiety adjacent to the acyl pocket, and the ethoxy group is aligned along the axis of the active site gorge. The stereochemistry of the nonaged tabun conjugate is R_P, and the electron density does not indicate any occupancy of the S_P enantiomer. In the absence of pseudorotation, attack of the phosphorus atom by Ser203 with the leaving group directed toward Asp74 leads to a stereochemical inversion of the phosphorus atom. In a study of *Electrophorus electricus* AChE (eAChE), it was found that (−)-tabun is 6.3 times more reactive than (+)-tabun (*41*). Assuming the stereochemical preference of the mouse enzyme is similar and unaffected by the crystal packing, the structure of the nonaged tabun conjugate reflects an enzyme mainly inhibited by S_P-(−)-tabun. The relatively small difference of the reactivity between the R_P and S_P enantiomers of tabun implicates that a fraction of the enzyme is in reality inhibited by R_P-(+)-tabun. However, due to the lack of any electron density of the less reactive enantiomer, it is not possible to estimate the relative fraction of the R_P and S_P enantiomers based exclusively on the diffraction data.

The nonaged tabun conjugate induces a structural change of the imidazole ring of His447 that moves toward Tyr337 and Phe338. In this position, a hydrogen bond between the His447 Nδ1 atom and a water molecule is achievable, whereas the distance is too large for a hydrogen bond between His447 and the tabun conjugate. Moreover, a structural change of the side chain of Phe338 toward Tyr124 is observed in the nonaged structure of mAChE inhibited by tabun. The displacements of Phe338 and His447 are reversible as demonstrated in the structure of mAChE in complex with an aged tabun conjugate. After the aging reaction, the side chains of Phe338 and His447 assume the conformation observed in the apo structure of mAChE. This places the imidazole ring of His447 in a favorable position for a strong hydrogen bond to the O2 oxygen of the tabun conjugate. The aged tabun conjugate is further coordinated with the O1 oxygen in the oxyanion hole, the O3 oxygen in the acyl pocket, and the ethoxy chain aligned along the axis of the active site gorge. The electron density of the ethoxy

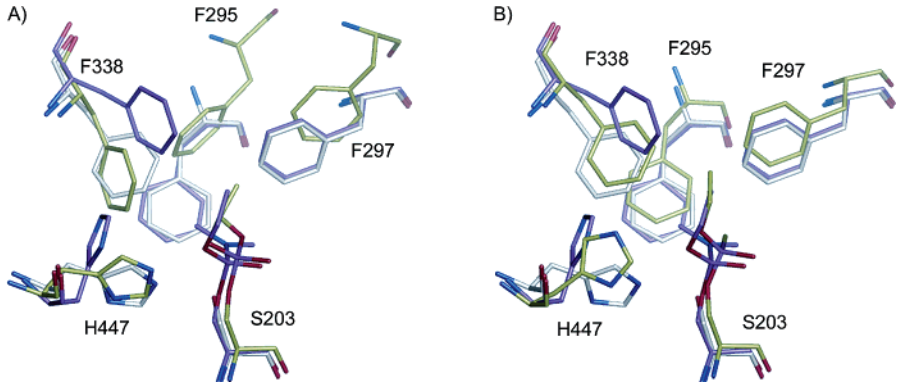

FIGURE 3: Structural alignment of the nonaged tabun conjugate shown in magenta, the apo form of mAChE in gray, and *Tc*AChE shown in green. The phosphorus atoms of the conjugates are shown in magenta, the oxygen atoms in red, and the nitrogen atoms in blue. (A) The structure of the aged DFP−*Tc*AChE conjugate (PDB entry 2DFP). (B) The structure of the nonaged VX−*Tc*AChE conjugate (PDB entry 1VXR).

chain is rather weak, and the atomic temperature factors of C3 and C4 are higher than the average of the protein chain, both observations symptomatic with a mobility of the ethoxy chain.

One can hypothesize that the structural changes of Phe338 and His447 are initiated by a steric clash between the side chain of Phe338 and the dimethylamine moiety of the nonaged tabun conjugate and that the displacement of His447 is a secondary, compensatory effect. In this hypothesis, the steric clash between Phe338 and the dimethylamine moiety is removed during the aging reaction, and the side chains of Phe338 and His447 are relaxed to the position found in the apo structure of mAChE. The close interaction between the imidazole ring of His447 and the phenyl ring of Phe338 has previously been studied in site-directed mutants of AChE (*42*). In the structure of *Tc*AChE inhibited by aged DFP the isopropyl group of the DFP conjugate is accommodated in the acyl pocket. This induces a significant disruption of Phe295 and Phe297 whereas only a negligible displacement of the side chain of Phe338 is observed (Figure 3) (*20*). Another possibility is that the structural change of Phe338 and His447 is a response to the electrostatic properties of the tabun conjugate that influence the conformation of His447. In this hypothesis, the distortion of Phe338 is an adaptive structural change that is necessary to accommodate the side chain of His447. The importance of the electrostatic properties has previously been emphasized in studies of *Tc*AChE inhibited by VX (*23*). However, in these studies, a less pronounced distortion was isolated to the side chain of His447 whereas Phe338 was unaffected (Figure 3). These differences may reveal a species-dependent diversity or reflect differences associated to the chemical properties of the VX versus tabun conjugates.

One can speculate that the distortion of His447 reflects a natural catalytic mobility, comparable to the mobility described for the active site His57 of α-lytic protease (*43*, *44*). Although a conformational heterogeneity of the side chain of His447 has been implied by proton NMR studies of AChE (*45*), it seems unlikely that the relatively large distortion observed in the nonaged structure of mAChE inhibited by tabun occurs during catalysis of the natural substrate. This is supported by the crystal structure of *Tc*AChE in complex with the transition state analogue inhibitor TMTFA that does not reveal any alternative conformation of His447 (*46*).

Studies of the aging reaction of tabun conjugates suggest a mechanism that proceeds through a P−N scission and replacement of the phosphoroamidoyl group by a water molecule (*18*). In this mechanism, a proton is transferred from His447 to the nitrogen of the phosphoroamidoyl moiety. A trigonal- bipyramidial intermediate is formed, and a pseudorotation orients the leaving group in the appropriate apical position from which it can be eliminated. During the pseudorotation, a rearrangement of the equatorial ligands of the trigonal bipyramid may occur (*47*). The orientation of the dimethylamine moiety in the acyl pocket is unfavorable for a protonation by His447, and the mechanism would require that His447 undergoes further, more extended structural changes to position the imidazole side chain in the vicinity of the N1 nitrogen. The protonation step could possibly involve a rotation of the tabun conjugate around the Ser203Oγ−P bond to place the dimethylamine moiety in the vicinity of His447. However, this seems unfavorable since this would disturb the extensive hydrogen-bonding network between the O1 oxygen of the tabun conjugate and the oxyanion hole. Furthermore, an extended rotation would place the ethoxy group under tight steric constraints in the oxyanion hole. The structure of the nonaged tabun conjugate does not offer any obvious clarification of the role of His447 during the aging mechanism of tabun. In fact, the O2 oxygen of the ethoxy group is in a better position than the dimethylamine moiety for a protonation by His447. Alternative mechanisms involving a secondary intramolecular protonation of the dimethylamine moiety cannot be excluded, and further studies are necessary to clarify the role of His447 with respect to the aging of tabun conjugates.

Structural barriers that prevent the reactivation of aged AChE−OP conjugates have been discussed earlier, and our data are in agreement with these observations (*20*, *23*, *24*). The delocalized formal negative charge of the aged tabun conjugate is stabilized by a strong hydrogen bond between the O2 oxygen of the tabun conjugate and His447 and by several hydrogen bonds between the O1 oxygen of the conjugate and the oxyanion hole. Moreover, the strong hydrogen bond between His447 and the O2 oxygen immobilizes the imidazole ring in an unproductive bond. The phosphonyl O3 oxygen is accommodated in the hydrophobic environment of the acyl pocket.

Acetylcholinesterase inhibited by tabun has proven very resistant to reactivation of most oximes that have been

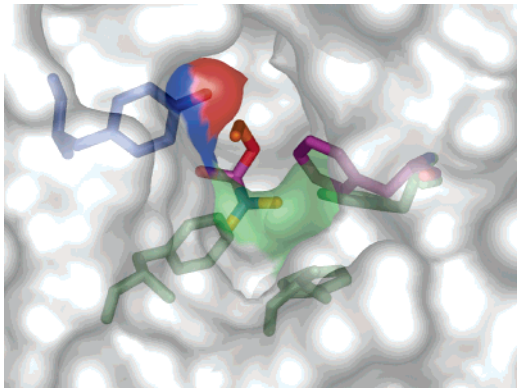

FIGURE 4: Surface representation of the apo form of mAChE viewed from the entrance of the active site gorge (PDB entry 1J06). The side chains of Phe295, Phe297, and Phe338 are shown in green whereas Tyr124 is shown in blue. A structural alignment of the nonaged tabun conjugate is shown in orange and magenta for the tabun conjugate and side chain of Phe338, respectively. The surface was calculated using the program Pymol (*49*).

studied (*6*, *7*). The structure of the nonaged tabun conjugate may offer some insights into this resistance. Studies of site-directed mutants of AChE have suggested that HI-6 attacks the phosphorus conjugate from the acyl pocket and that steric constraints within this region affect the efficiency of reactivators (*9*, *25*, *48*). The observed conformation of Phe338 positions parts of the phenyl ring in the narrow active site gorge (Figure 4). This will probably negatively affect the ease of access to the acyl pocket for the HI-6 molecule. The hypothesis may also explain the fact that reactivators with the oxime functionality in the 4-position of the pyridinium ring are generally better reactivators of tabun-inhibited AChE than reactivators with the oxime functionality in the 2-position (*10*). Reactivators with the oxime functionality in the 4-position are less bulky than the corresponding 2-substituted oxime and supposedly more suitable to adopt a proper attacking position. However, the decreased dimensions of the active site gorge are probably not the only factor that contributes to the resistance of tabun conjugates toward reactivation, and further studies are necessary to investigate this resistance.

ACKNOWLEDGMENT

We thank Dr. Yngve Cerenius for assistance at the beam line I711 at MAX laboratory. The authors also acknowledge Dr. Gertrud Puu, Dr. Göran Bucht, and Elisabet Artursson for valuable discussions throughout the study.

SUPPORTING INFORMATION AVAILABLE

Two figures showing a plot of the initial rate at different substrate concentrations with the corresponding Lineweaver−Burk plot inserted of purified AChE and AChE derived from dissolved crystals and silver-stained SDS−PAGE showing standard molecular weights, AChE expressed in FreeStyle medium, purified AChE, noninhibited, dissolved crystals (control sample), and dissolved, inhibited AChE. This material is available free of charge via the Internet at http://pubs.acs.org.

REFERENCES

1. Sussman, J. L., Harel, M., Frolow, F., Oefner, C., Goldman, A., Toker, L., and Silman, I. (1991) Atomic structure of acetylcholinesterase from *Torpedo californica*: a prototypic acetylcholine-binding protein, *Science 253*, 872−879.
2. Nagao, M., Takatori, T., Matsuda, Y., Nakajima, M., Iwase, H., and Iwadate, K. (1997) Definitive evidence for the acute sarin poisoning diagnosis in the Tokyo subway, *Toxicol. Appl. Pharmacol. 144*, 198−203.
3. Macilwain, C. (1993) Study proves Iraq used nerve gas, *Nature 363*, 3.
4. Kwong, T. C. (2002) Organophosphate pesticides: biochemistry and clinical toxicology, *Ther. Drug Monit. 24*, 144−149.
5. Gunnell, D., and Eddleston, M. (2003) Suicide by intentional ingestion of pesticides: a continuing tragedy in developing countries, *Int. J. Epidemiol. 32*, 902−909.
6. Worek, F., Thiermann, H., Szinicz, L., and Eyer, P. (2004) Kinetic analysis of interactions between human acetylcholinesterase, structurally different organophosphorus compounds and oximes, *Biochem. Pharmacol. 68*, 2237−2248.
7. Kuca, K., and Kassa, J. (2003) A comparison of the ability of a new bispyridinium oxime−1-(4-hydroxyiminomethylpyridinium)-4-(4-carbamoylpyridinium)butane dibromide and currently used oximes to reactivate nerve agent-inhibited rat brain acetylcholinesterase by in vitro methods, *J. Enzyme Inhib. Med. Chem. 18*, 529−535.
8. Taylor, P., Wong, L., Radic, Z., Tsigelny, I., Bruggemann, R., Hosea, N. A., and Berman, H. A. (1999) Analysis of cholinesterase inactivation and reactivation by systematic structural modification and enantiomeric selectivity, *Chem.-Biol. Interact. 119−120*, 3−15.
9. Wong, L., Radic, Z., Bruggemann, R. J., Hosea, N., Berman, H. A., and Taylor, P. (2000) Mechanism of oxime reactivation of acetylcholinesterase analyzed by chirality and mutagenesis, *Biochemistry 39*, 5750−5757.
10. Cabal, J., Kuca, K., and Kassa, J. (2004) Specification of the structure of oximes able to reactivate tabun-inhibited acetylcholinesterase, *Basic Clin. Pharmacol. Toxicol. 95*, 81−86.
11. Benschop, H. P., and Keijer, J. H. (1966) On the mechanism of aging of phosphonylated cholinesterases, *Biochim. Biophys. Acta 128*, 586−588.
12. Michel, H. O., Hackley, B. E., Jr., Berkowitz, L., List, G., Hackley, E. B., Gillilan, W., and Pankau, M. (1967) Ageing and dealkylation of Soman (pinacolylmethylphosphonofluoridate)-inactivated eel cholinesterase, *Arch. Biochem. Biophys. 121*, 29−34.
13. Viragh, C., Kovach, I. M., and Pannell, L. (1999) Small molecular products of dealkylation in soman-inhibited electric eel acetylcholinesterase, *Biochemistry 38*, 9557−9561.
14. Harris, L. W., Fleisher, J. H., Clark, J., and Cliff, W. J. (1966) Dealkylation and loss of capacity for reactivation of cholinesterase inhibited by sarin, *Science 154*, 404−407.
15. Jennings, L. L., Malecki, M., Komives, E. A., and Taylor, P. (2003) Direct analysis of the kinetic profiles of organophosphate-acetylcholinesterase adducts by MALDI-TOF mass spectrometry, *Biochemistry 42*, 11083−11091.
16. Ordentlich, A., Kronman, C., Barak, D., Stein, D., Ariel, N., Marcus, D., Velan, B., and Shafferman, A. (1993) Engineering resistance to "aging" of phosphylated human acetylcholinesterase. Role of hydrogen bond network in the active center, *FEBS Lett. 334*, 215−220.
17. Shafferman, A., Ordentlich, A., Barak, D., Stein, D., Ariel, N., and Velan, B. (1996) Aging of phosphylated human acetylcholinesterase: catalytic processes mediated by aromatic and polar residues of the active centre, *Biochem. J. 318* (Part 3), 833−840.
18. Barak, D., Ordentlich, A., Kaplan, D., Barak, R., Mizrahi, D., Kronman, C., Segall, Y., Velan, B., and Shafferman, A. (2000) Evidence for P-N bond scission in phosphoroamidate nerve agent adducts of human acetylcholinesterase, *Biochemistry 39*, 1156−1161.
19. Hosea, N. A., Berman, H. A., and Taylor, P. (1995) Specificity and orientation of trigonal carboxyl esters and tetrahedral alkylphosphonyl esters in cholinesterases, *Biochemistry 34*, 11528−11536.
20. Millard, C. B., Kryger, G., Ordentlich, A., Greenblatt, H. M., Harel, M., Raves, M. L., Segall, Y., Barak, D., Shafferman, A., Silman, I., and Sussman, J. L. (1999) Crystal structures of aged phosphonylated acetylcholinesterase: nerve agent reaction products at the atomic level, *Biochemistry 38*, 7032−7039.
21. de Jong, L. P., and Wolring, G. Z. (1978) Effect of 1-(AR)alkyl-2-hydroxyiminomethyl-pyridinium salts on reactivation and aging of acetyl-cholinesterase inhibited by ethyl dimethylphosphoramidocyanidate (tabun), *Biochem. Pharmacol. 27*, 2229−2235.

22. Elhanany, E., Ordentlich, A., Dgany, O., Kaplan, D., Segall, Y., Barak, R., Velan, B., and Shafferman, A. (2001) Resolving pathways of interaction of covalent inhibitors with the active site of acetylcholinesterases: MALDI-TOF/MS analysis of various nerve agent phosphyl adducts, *Chem. Res. Toxicol. 14*, 912−918.
23. Millard, C. B., Koellner, G., Ordentlich, A., Shafferman, A., Silman, I., and L., S. J. (1999) Reaction products of acetylcholinesterase and VX reveal a mobile histidine in the catalytic triad, *J. Am. Chem. Soc. 121*, 9883−9884.
24. Nachon, F., Asojo, O. A., Borgstahl, G. E., Masson, P., and Lockridge, O. (2005) Role of water in aging of human butyrylcholinesterase inhibited by echothiophate: the crystal structure suggests two alternative mechanisms of aging, *Biochemistry 44*, 1154−1162.
25. Kovarik, Z., Radic, Z., Berman, H. A., Simeon-Rudolf, V., Reiner, E., and Taylor, P. (2004) Mutant cholinesterases possessing enhanced capacity for reactivation of their phosphonylated conjugates, *Biochemistry 43*, 3222−3229.
26. Saxena, A., Maxwell, D. M., Quinn, D. M., Radic, Z., Taylor, P., and Doctor, B. P. (1997) Mutant acetylcholinesterases as potential detoxification agents for organophosphate poisoning, *Biochem. Pharmacol. 54*, 269−274.
27. Ashani, Y., Radic, Z., Tsigelny, I., Vellom, D. C., Pickering, N. A., Quinn, D. M., Doctor, B. P., and Taylor, P. (1995) Amino acid residues controlling reactivation of organophosphonyl conjugates of acetylcholinesterase by mono- and bisquaternary oximes, *J. Biol. Chem. 270*, 6370−6380.
28. Grosfeld, H., Barak, D., Ordentlich, A., Velan, B., and Shafferman, A. (1996) Interactions of oxime reactivators with diethylphosphoryl adducts of human acetylcholinesterase and its mutant derivatives, *Mol. Pharmacol. 50*, 639−649.
29. Bourne, Y., Taylor, P., and Marchot, P. (1995) Acetylcholinesterase inhibition by fasciculin: crystal structure of the complex, *Cell 83*, 503−512.
30. Marchot, P., Ravelli, R. B., Raves, M. L., Bourne, Y., Vellom, D. C., Kanter, J., Camp, S., Sussman, J. L., and Taylor, P. (1996) Soluble monomeric acetylcholinesterase from mouse: expression, purification, and crystallization in complex with fasciculin, *Protein Sci. 5*, 672−679.
31. Ellman, G. L., Courtney, K. D., Andres, V., Jr., and Feather-Stone, R. M. (1961) A new and rapid colorimetric determination of acetylcholinesterase activity, *Biochem. Pharmacol. 7*, 88−95.
32. Levy, D., and Ashani, Y. (1986) Synthesis and in vitro properties of a powerful quaternary methylphosphonate inhibitor of acetylcholinesterase. A new marker in blood-brain barrier research, *Biochem. Pharmacol. 35*, 1079−1085.
33. Kabsch, W. (1993) Automatic processing of rotation diffraction data from crystals of initially unknown symmetry and cell constants, *J. Appl. Crystallogr. 26*, 795−800.
34. Kabsch, W. (1988) Evaluation of single-crystal X-ray diffraction data from a position-sensitive detector, *J. Appl. Crystallogr. 21*, 916−924.
35. Bourne, Y., Taylor, P., Radic, Z., and Marchot, P. (2003) Structural insights into ligand interactions at the acetylcholinesterase peripheral anionic site, *EMBO J. 22*, 1−12.
36. Murshudov, G. N., Vagin, A. A., and Dodson, E. J. (1997) Refinement of macromolecular structures by the maximum-likelihood method, *Acta Crystallogr., Sect. D: Biol. Crystallogr. D53*, 240−255.
37. Brunger, A. T. (1992) Free *R* value: a novel statistical quantity for assessing the accuracy of crystal structures, *Nature 355*, 472−474.
38. Jones, T. A., Zou, J. Y., Cowan, S. W., and Kjeldgaard (1991) Improved methods for building protein models in electron density maps and the location of errors in these models, *Acta Crystallogr., Sect. A 47* (Part 2), 110−119.
39. Laskowski, R. A., MacArthur, M. W., Moss, D. S., and Thornton, J. M. (1993) PROCHECK: a program to check the stereochemical quality of protein structures, *J. Appl. Crystallogr. 26*, 283−291.
40. Vriend, G. (1990) WHAT IF: A molecular modelling and drug design program, *J. Mol. Graphics Modelling 8*, 52−56.
41. Degenhardt, C. E. A. M., Van Den Berg, G. R., De Jong, L. P. A., and Benschop, H. P. (1986) Enantiospecific complexation gas chromatography of nerve agents. isolation and properties of the enantiomers of ethyl *N*,*N*-dimethylphosphoramidocyanidate, *J. Am. Chem. Soc. 108*, 8290−8291.
42. Barak, D., Kaplan, D., Ordentlich, A., Ariel, N., Velan, B., and Shafferman, A. (2002) The aromatic "trapping" of the catalytic histidine is essential for efficient catalysis in acetylcholinesterase, *Biochemistry 41*, 8245−8252.
43. Bone, R., Sampson, N. S., Bartlett, P. A., and Agard, D. A. (1991) Crystal structures of alpha-lytic protease complexes with irreversibly bound phosphonate esters, *Biochemistry 30*, 2263−2272.
44. Haddad, K. C., Sudmeier, J. L., Bachovchin, D. A., and Bachovchin, W. W. (2005) alpha-lytic protease can exist in two separately stable conformations with different His57 mobilities and catalytic activities, *Proc. Natl. Acad. Sci. U.S.A. 102*, 1006−1011.
45. Massiah, M. A., Viragh, C., Reddy, P. M., Kovach, I. M., Johnson, J., Rosenberry, T. L., and Mildvan, A. S. (2001) Short, strong hydrogen bonds at the active site of human acetylcholinesterase: proton NMR studies, *Biochemistry 40*, 5682−5690.
46. Harel, M., Quinn, D. M., Haridasan, K. N., Silman, I., and Sussman, J. L. (1996) The X-ray structure of a transition state analogue complex reveals the molecular origins of the catalytic power and substrate specificity of acetylcholinesterase, *J. Am. Chem. Soc. 118*, 2340−2346.
47. Berry, R. S. (1960) Correlation of rates of intramolecular tunneling processes, with application to some group V cCompounds, *J. Chem. Phys. 32*, 933−938.
48. Luo, C., Leader, H., Radic, Z., Maxwell, D. M., Taylor, P., Doctor, B. P., and Saxena, A. (2003) Two possible orientations of the HI-6 molecule in the reactivation of organophosphate-inhibited acetylcholinesterase, *Biochem. Pharmacol. 66*, 387−392.
49. DeLano, W. L. (2002) The PyMOL Molecular Graphics System, DeLano Scientific, San Carlos, CA.

BI051286T